JOURNAL OF CATALYSIS 97, 437–447 (1986)

Crystallographic Structure and Chemisorption Activity of Palladium/Mica Model Catalysts

II. Temperature Programmed Desorption Study of CO Chemisorption on Well-Defined Palladium Particles

E. GILLET, S. CHANNAKHONE, AND V. MATOLIN[1]

Laboratoire de Microscopie et Diffractions Electroniques, U.A. 797, Faculté des Sciences et Techniques de Saint-Jérôme, Rue Henri Poincaré, 13397 Marseille Cedex 13, France

Received July 20, 1984; revised July 23, 1985

Temperature-programmed desorption (TPD) has been used to investigate binding states of CO on well-defined particles of Pd in the size range 2–20 nm. The morphology and area for a given size are deduced from transmission electron microscopy (TEM) observations as described by M. F. Gillet and S. Channakhone (*J. Catal.* **97**, 427 (1986)). It is shown that small particles exhibit two CO binding states, and one of them is suggested to be related to edge sites. Evidence of CO dissociation on smaller particles is reported from coverage measurements. High sticking coefficient values are interpreted assuming a CO diffusion process on the mica support.

INTRODUCTION

CO chemisorption on Group VIII metals is one of the best-known adsorption systems, and one may find in the literature many papers devoted to the interaction of CO with various single crystal surfaces of palladium, e.g., Refs. (*1–8*) in Part I (*1*). Thus we shall not try to review all the available data, but will only cite the results relevant to discussing our work.

Some authors have recently studied the chemisorption behavior of supported metallic particles and examined the size effects in catalysis. In this field we note the experiments carried out on supported Pd and Ni particles by Poppa *et al.* (*2–6*). These authors show that molecular adsorption of CO occurs in two states and that thermal desorption is accompanied by dissociation with a rate depending on the particle size. Residual carbon has a poisoning effect on the CO oxidation. More recently, Zhu and Schmidt characterized Pd–Rh alloys by CO chemisorption (*7*). They pointed out that very small particles produce "higher CO binding states" than do the larger particles. Moreover, they showed that O_2 treatments suppress CO adsorption on Rh. Furthermore Takasu *et al.* (*8*) observed, by XPS, changes in the Pd valence band as a function of increasing particle size in a Pd/SiO_2 system. Toolenaar *et al.* (*9*) observed a size effect in the IR absorption band frequency of CO adsorbed on Ir/Al_2O_3. They found for decreasing particle size an increasing number of CO molecules in a state attributed by the authors to molecules in stronger interaction with metal.

In this paper we report results obtained by thermal desorption of CO on well-defined Pd particles. We shall discuss the adsorption features (number and nature of the adsorption states, binding energy, and the CO dissociation) on the base of the size and the surface structure of the particles.

[1] Permanent address: Department of Electronics and Vacuum Physics, Charles University, Povltavska 1, 18000 Prague 8, Czechoslovakia.

0021-9517/86 $3.00

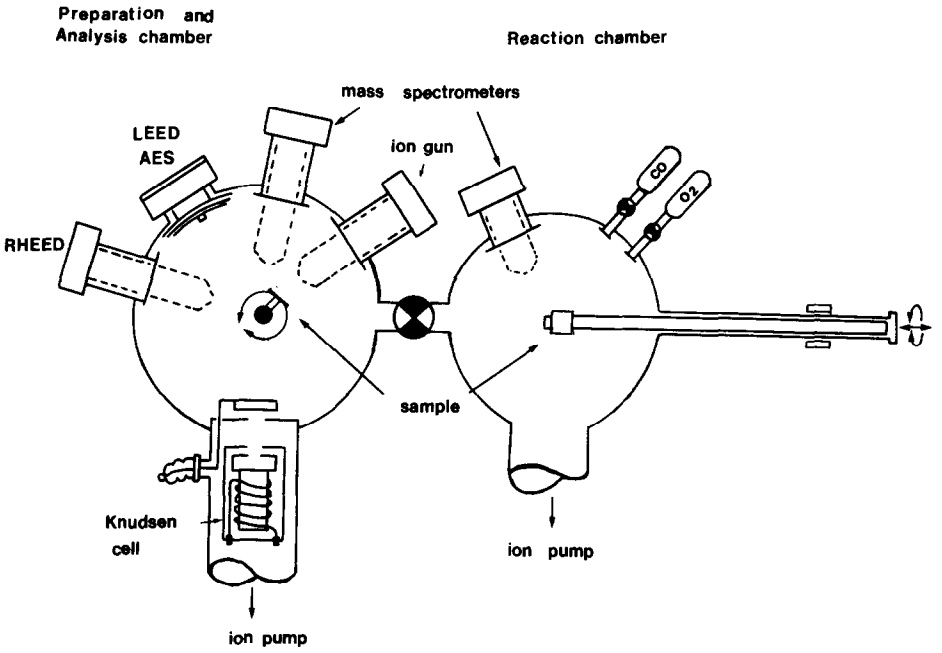

FIG. 1. The two-chamber UHV system allowing sample preparation, surface characterization, and reactions.

EXPERIMENTAL

a. Preparation and Characterization of the Samples

For these studies we built a special two-chamber UHV system (*10*). The two chambers can be isolated from one another and separately ion pumped to a base pressure in the range 10^{-7}–10^{-8} Pa (Fig. 1).

The preparation chamber was used to prepare well-defined model catalysts and to perform Auger electron spectroscopy (AES) and secondary ion mass spectrometry (SIMS) control experiments. Palladium particles are grown on a UHV heat-treated mica cleavage following a process giving reproducible conditions (*10*). The cleanliness and crystallographic structure of mica substrates are checked by AES-LEED analysis before metal deposition.

The palladium source is a Knudsen cell and the atomic flux is monitored as described in Part I (*1*). The growing conditions are selected to achieve average particle sizes between 2 and 12 nm (substrate temperature, 573 K; metallic flux, 1.7 × 10^{13} atoms cm^{-2} s^{-1}; deposition time, in the range 1–7 min).

A special substrate holder permits both a transfer process of the sample between the two chambers and a programmable radiative heating. Temperatures and heating rates are approximated from previous calibrations obtained by attaching a thermocouple to the mica surface with silver paste.

Heat transfer between the mica substrate and the metallic deposit was carefully taken into account. Heating rates are thus determined in each experimental situation of mica cleavage thickness and initial sample temperature T_0.

The as-deposited sample is transferred to the reaction chamber for temperature-programmed desorption (TPD) studies. An experimental run starts with the stabilization of the particles by annealing in a CO + O_2 mixture. As was pointed out in Part I (*1*), it is possible to obtain suitable model catalysts by heating at T = 573 K in a CO + O_2 mixture (P_{CO}/P_{O_2} = 0.1 for a total pressure of about 10^{-4} Pa) for 1 h.

Such treatment produces particles with

TABLE 1

Main Features of Pd/Mica Particle Samples Used in TPD Experiments

Sample number	$N \times 10^{11}$ (cm^{-2})	Mean diameter, ϕ (nm)	Epitaxial orientations	Morphology
1	4.5	1.2	Nonoriented	Spherical
2	4	1.5	Nonoriented + few (111) + (110)	Spherical
3	9.7	2.5	Nonoriented 50% + (111) + (110) 5	Spherical + cuboctahedral + few icosahedral
4	5.2	3.3	(111) 50% (110) 50%	Half-cuboctahedral
5	5	4	(111) 60% (110) 40%	Half-cuboctahedral
6	7.86	5.5	(111) 60% (110) 40%	Half-cuboctahedral
7	5.4	6.5	(111) 80% (110) 20%	Triangular plates truncated tetrahedral half-sphere
8	1.6	7	(111) + few (110)	
9	1.97	7.6	(111) + few (110)	
10	2.8	9	(111)	

shapes and orientations depending on the size. The main features of the Pd particles (density, mean diameter ϕ, morphology, orientation) are summarized in Table 1 for the samples used in the chemisorption experiments.

b. TPD Experiments

Thermal CO desorption spectra are obtained for various exposures at a substrate temperature of 300 K $\leq T \leq$ 350 K in a CO pressure range of 10^{-4}–10^{-6} Pa from 0.1 L until complete saturation (~5 L) of the surface particles is reached. During heating, four gas peaks (typically CO, O_2, H_2O, and CO_2) can be monitored and stored as a function of time by a data acquisition system linked to a quadrupole mass spectrometer. The amounts of O_2, H_2O, and CO_2 remain at the background pressure level during TPD runs if samples are prepared as described in Part I (*1*). TPD spectra can then be separately recorded on an x–y plotter. A heating rate of 6–7 K s^{-1} was applied during TPD measurements. Under these conditions desorption spectra occur in the range 400–673 K.

RESULTS

CO Desorption Kinetics as a Function of Particle Size

Figures 2–4 show typical TPD spectra obtained as a function of exposure for samples 1–10 (Table 1). The spectra are given as a function of time because each spectrum has its own temperature scale (*10*) which was used to perform interpretations.

In Table 2 we report coverages and temperatures of the maxima of peaks for the spectra in Figs. 3 and 4.

The features of the spectra in Figs. 2–4 are qualitatively the same. For the lower exposures CO desorption leads to a single peak (peak 1). With increasing exposures a shoulder appears on the lower temperature side of peak 1. This shoulder gives rise to the second peak (peak 2) which is well defined only for the smaller particles (Figs. 2 and 3).

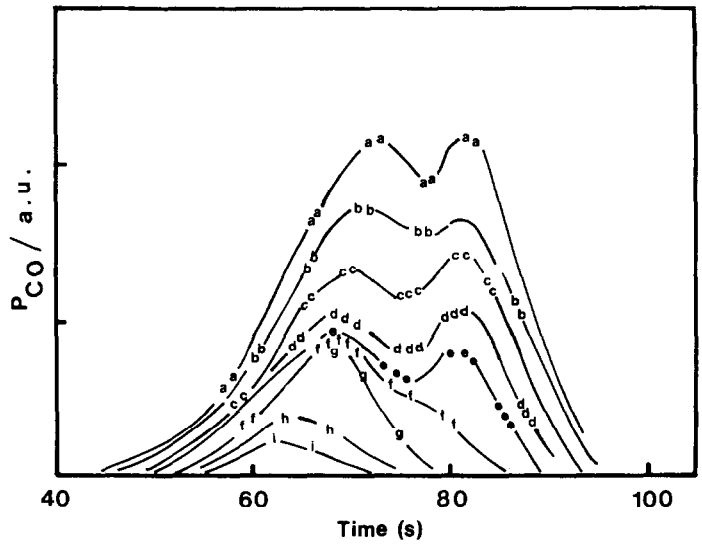

FIG. 2. TPD spectra for CO from Pd particles (mean particle size = 2 nm). Exposures were (a) 6 L, (b) 4 L, (c) 3 L, (d) 1 L, (e) 5 L, (f) 4 L, (g) 0.2 L, (h) 0.1 L, (i) 0.05 L [L = Langmuir, 1 L = 10^{-6} Torr × s].

Peak 1 begins to fill first and saturates at about 3 L exposure. Its relative population decreases when the particle size increases. The ratio of the area under the saturated peak 1 to the total area of the desorption spectrum is plotted versus the particle size in Fig. 5.

TABLE 2

Maximum Temperatures of the TPD Spectra in Figs. 3 and 4, Showing Slight Shift toward Lower Temperature with Increasing Coverage

Coverage, θ	Spectra from Fig. 3		Spectra from Fig. 4 T_M (K)
	T_{M_1} (K)	T_{M_2} (K)	
0.01	—	—	453
0.02	466	—	453
0.03	466	—	452
0.04	—	—	452
0.06	465	—	—
0.07	463	—	452
0.08	463	—	—
0.09	463	—	452
0.10	460	452	—
0.13	460	452	451
0.15	460	451	—
0.20	460	451	—
0.25	—	—	450
0.34	—	—	449
0.45	460	451	—
0.56	460	451	—
0.6	—	—	449

By comparison with CO chemisorption on single crystal surfaces, these two peaks can be interpreted on the basis of distinct species adsorbed on different sites and/or in terms of adsorption with precursor states (*12, 13*). In addition the possibility of lateral interactions between chemisorbed species (mainly dissociative adsorption) should be considered.

Rate expressions were derived for adsorption and desorption using the above hypothesis (*14, 15*), which could be adapted for CO chemisorption on metallic particles. These rate expressions are complex and involve a large number of parameters to fit TPD spectra from Pd particles. The analysis of Figs. 2–4 by such a method remained quite impossible.

Thus, the activation energy for desorption E_d was determined using a treatment based on variable desorption rates for constant coverages (*16*). The results are plotted versus coverage (*4*) (Fig. 6) for two samples corresponding to particles with mean diameters of 3.5 and 6.6 nm. For the

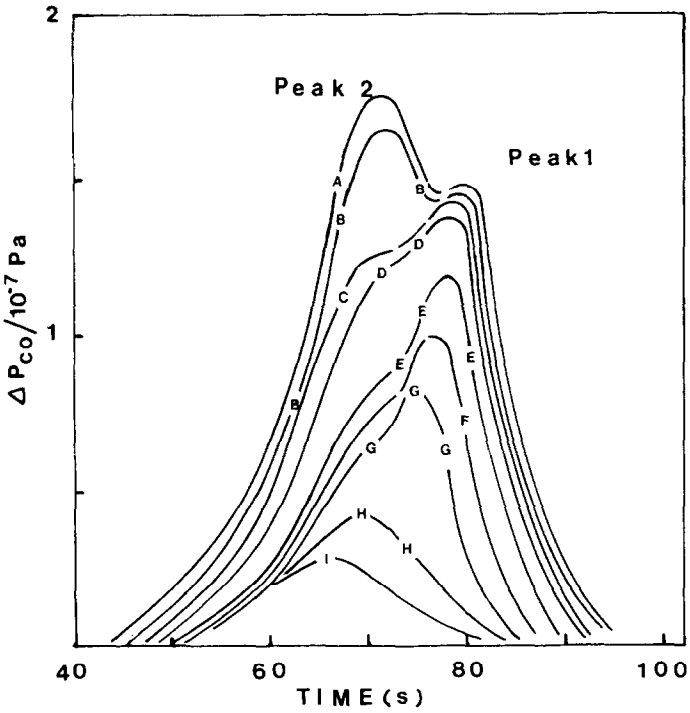

FIG. 3. TPD spectra for CO from Pd particles (size = 4 nm). Exposures were (A) 5 L, (B) 4 L, (C) 2 L, (D) 1.5 L, (E) 1 L, (F) 0.7 L, (G) 0.6 L, (H) 0.25 L, (I) 0.2 L.

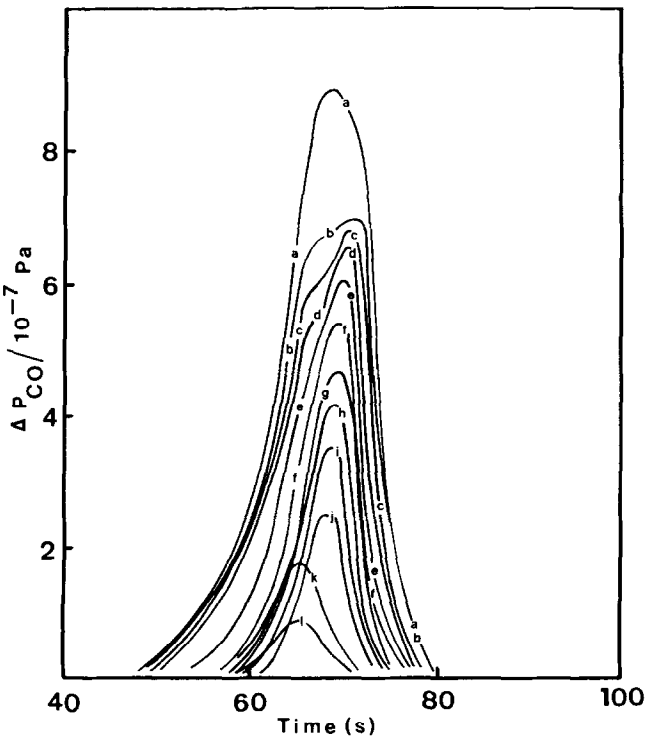

FIG. 4. TPD spectra for CO from Pd particles (size = 6 nm). Exposures were (a) 7 L, (b) 4 L, (c) 3 L, (d) 1.5 L, (e) 1 L, (f) 0.7 L, (g) 0.5 L, (h) 0.4 L, (i) 0.35 L, (j) 0.25 L, (k) 0.2 L, (l) 0.1 L.

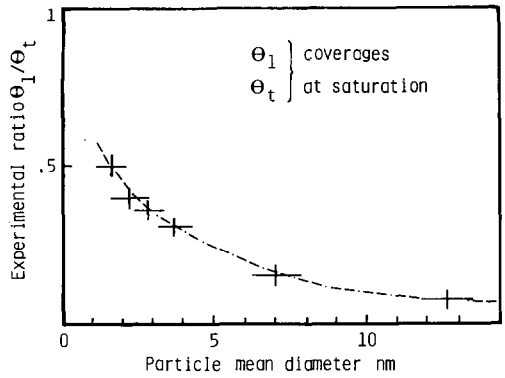

FIG. 5. Experimental ratio θ_1/θ_t between saturation coverages plotted versus particle size. θ_1 is the coverage in the high-energy state (peak 1). θ_t is the total coverage.

large particles (ϕ = 6.6 nm) E_d exhibits an important and continuous decrease as the coverage increases, probably due to strong interactions between adsorbed CO molecules.

For the small particles (ϕ = 3.5 nm) E_d maintains a rather constant value of about 38 kcal mol^{-1} for $\theta < 0.5\theta_{max}$. We generally observed such behavior for particles with $\phi < 5$ nm; moreover, it is important to note that the E_d values are always higher for small particles than for large ones. This is mainly evident for $\theta < 0.5\theta_{max}$.

CO Adsorption Kinetics: Initial Sticking Coefficient

From TPD spectra we deduced the adsorption kinetics $\theta(t)$ (*17*)—coverage versus time—and after differentiation sticking coefficients, $s(\theta)$ (i.e., the adsorption probability of one impinging CO molecule). The values of s are plotted in Figs. 7a–c as a function of coverage for samples 3, 5, and 7 of Table 1. As a comparison we plotted, on the same figure, $s(\theta)$ for a continuous thin (111) film of Pd (Fig. 7d).

These curves emphasize three important features:

(1) The values of the initial sticking coefficient $s_0 = s\ (\theta = 0)$ are obviously too large ($1.7 \leq s_0 \leq 9$).

(2) s_0 decreases with the mean particle diameter.

(3) The variations $s(\theta)$ for particles and the (111) surface exhibit quite similar outlines, namely, a plateau for smaller coverages followed by a slow decrease. This be-

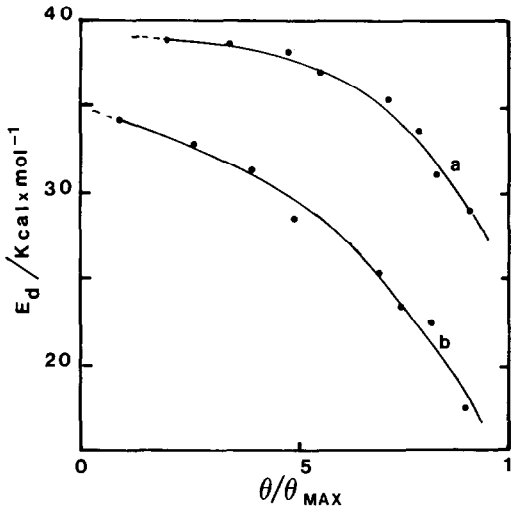

FIG. 6. Activation energy for CO desorption from Pd particles versus coverage in two cases: (a) mean particle diameter lower than 5 nm, (b) mean particle diameter higher than 5 nm.

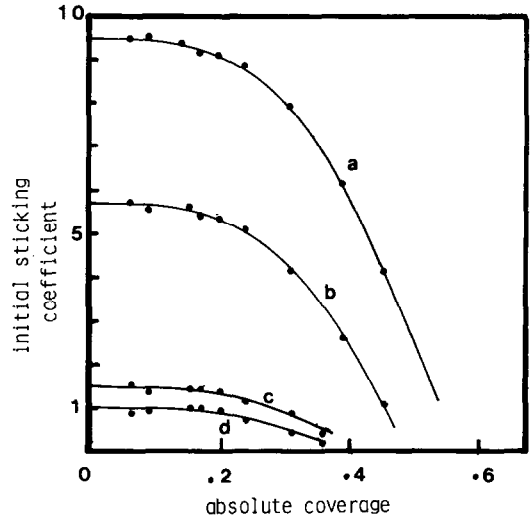

FIG. 7. CO sticking coefficients versus absolute coverages for various particle sizes: (a) 2.5 nm, (b) 4 nm, (c) 6.5 nm, (d) continuous Pd film.

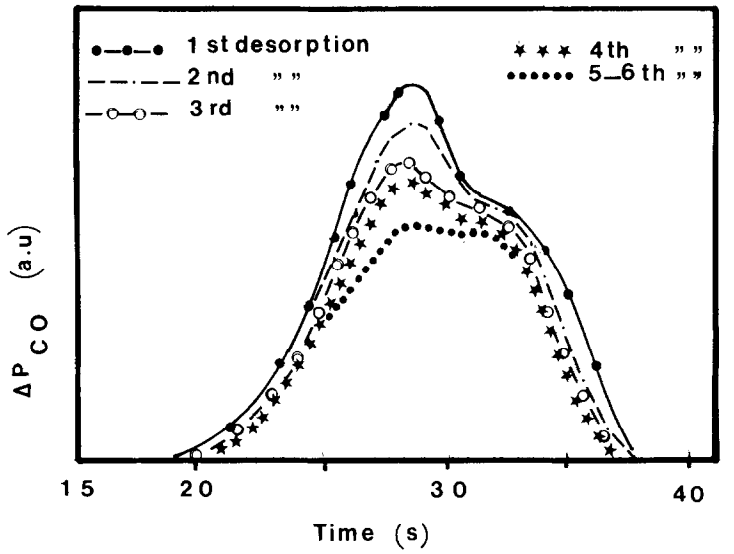

FIG. 8. TPD spectra as obtained after saturation exposure for six successive adsorption–desorption sequences (see text).

havior is generally attributed to adsorption kinetics involving a precursor state (*17*).

We will explain points 1 and 2 in the Discussion. One can, however, point out that in the case of CO adsorption on a continuous surface, s_0 calculations have given a more realistic value ($s_0 \simeq 1$). Therefore the accuracy of pressure measurements cannot be suspected.

On the other hand, atomic surface densities for particles were calculated taking account of the particle morphology and density as reported in Table 1. Thus errors in coverage values cannot be responsible for features (1) and (2) which would have a physical meaning.

Carbon Contamination of Small Pd Particles

After each TPD sequence the area S of the saturation spectrum decreases (Fig. 8). We have reported in Fig. 9 the ratio S_N/S_1 as a function of the desorption run number N for various samples (S_N is the desorption peak area for the number in series N). Curves a and b concern particles grown under the same conditions but which are respectively as-deposited, and after treatment in a CO + O_2 atmosphere. Curves c and d (Fig. 9) correspond to stabilized particles with mean diameters of 3 and 4 nm, respectively.

It can be seen that the decay in the desorption peak area depends strongly on particle size: the amount of adsorbed CO decreases all more rapidly when the particle size is smaller. This phenomenon was pre-

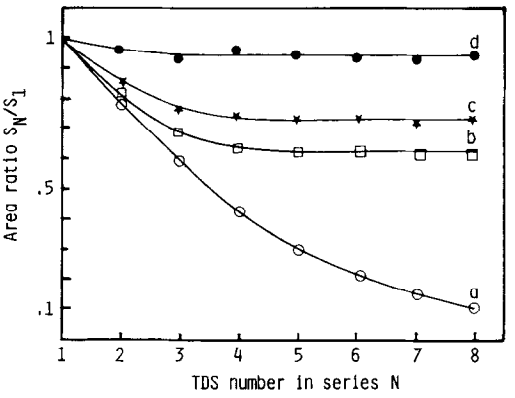

FIG. 9. TPD spectra area plotted against the series number N of the adsorption–desorption sequence for (a) as-deposited particles, (b) as-deposited particles after stabilization (mean diameter 2.5 nm), (c) stabilized particles (mean diameter 3 nm), (d) stabilized particles (mean diameter 6 nm).

viously pointed out (*5*) and was attributed to a carbon contamination resulting from CO dissociation. However, comparison of curves a and b in Fig. 9 shows that this effect is not entirely due to carbon contamination but also depends on the stabilization of particles. Thus the high rate of the decrease in curve a must be attributed to both particle coalescence and rebuilding.

The S_N/S_1 values plotted in curves b–d in Fig. 9 were obtained on stabilized particles; they decrease rapidly during the first three desorption runs and much more slowly in the later ones. An analysis by AES and SIMS confirmed the presence of carbon on the small stabilized particle surface (*18*). Thus, this phenomenon cannot be entirely attributed to morphological changes which could occur during a thermal desorption experiment and we must consider that the poisoning effect of Pd particles by carbon is real.

The hypothesis of CO decomposition during desorption is easy to correlate with the adsorption mechanism when it is governed by dissociation, as in the case of the CO–Ni system. Dissociation of CO has never been observed on bulk Pd surfaces. However, taking into account the above results we considered that special sites present on small particles only (e.g., edge atoms) would promote dissociative adsorption. The resulting carbon contamination would affect the related desorption peak. This feature, however, is not evident in Fig. 8. Successive desorption spectra exhibit a decrease of their whole area during the contamination process. Thus the problem will not be solved by TPD experiments only. We anticipate that static SIMS investigations will give more information about the CO–Pd bonding.

DISCUSSION

The TPD study of CO chemisorption on Pd particles reveals two important features associated with small particle size, namely, the presence of two desorption peaks and a relatively high bonding energy for CO molecules adsorbed in the low coverage domain. It may be attractive to correlate the two results with the particle shapes which are, for small sizes ($\theta < 5$ nm), mostly cuboctahedral and which exhibit (111) and (100) faces. However, this hypothesis does not agree with the heat of adsorption values which are approximately equal for CO on bulk Pd (111) and Pd(100) (*3, 19*).

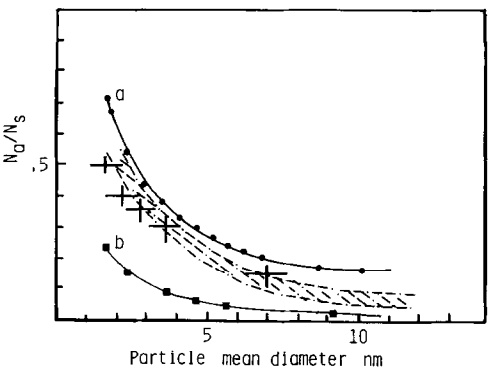

FIG. 10. N_a/N_s ratio versus particle size (N_a = number of edge atoms, N_s = total number of surface atoms) for half-cuboctahedra in (110) orientation (curve a) and for half-truncated spheres in (111) orientation; particle thickness = two-thirds of sphere radius (curve b). Crosses indicate the experimental values of relative amounts of CO adsorbed in TPD peak 1 (see Fig. 5).

We cannot exclude small facets (110) on the top of small particles giving strong CO bonding (for CO on Pd (110), $E_d \simeq 40$ kcal mol^{-1} (*19*)). In this case, these facets would have a small area and would contribute very little to adsorption.

On the other hand, we might also assume that edge atoms have intrinsic properties. Let us suppose that particles are half-cuboctahedra for small sizes and truncated spheres for large sizes. We calculate the ratio N_a/N_s as a function of particle size (N_a = number of edge atoms, N_s = total number of surface atoms). Taking into account, for the various particle orientations, their relative proportion and the size dispersion, the ratio N_a/N_s is represented by a dashed area (Fig. 10). We have also reported in Fig. 10 the experimental values of the ratio of the number of molecules adsorbed in state 1 to

the total number of adsorbed molecules. It is easy to see that the relative number of CO molecules adsorbed in the high temperature state is in rather good agreement with the ratio N_a/N_s. This indicates that adsorption with a high bonding energy, corresponding to the high temperature TPD peak, can be related to edge atoms; the other peak is then attributed to adsorption on faces.

From this point of view, the occurrence of two bonding states is not correlated with a particular particle orientation induced by a given substrate. On the other hand, they are characteristic of small particles which show a large tendency to exhibit facets and edges after heating in a CO + O_2 gas mixture.

Moreover, large E_d values are always observed for the smaller particles. Toolenaar *et al.* (*9*) and Zhu and Schmidt (*7*) obtained similar results with other metals, by IR measurements and TPD, respectively; they point out that when the particle size decreases, the bonding energy of CO increases. The authors suggested that the higher bonding state is associated with high free energy planes (for example (110) planes). As shown in Part I (*1*), the TEM results did not give proof of the existence of such planes in the case of small particles. On the contrary, we observed mainly low energy planes ((111) planes). Thus the properties of small particles with regard to CO chemisorption could be explained by the existence of active sites such as edge sites.

Another small size effect is pointed out above with the large value of the initial sticking coefficient s ($\theta = 0$). To explain this effect we supposed that CO molecules impinging on the bare mica surface can reach Pd particles by surface diffusion. Under our experimental conditions the diffusion of CO molecules on mica toward a Pd particle obeys the equation

$$\lambda^2 \left(\frac{d^2\varphi}{dr^2} + \frac{1}{r}\frac{d\varphi}{dr}\right) - \varphi = 0 \qquad (1)$$

where $\varphi(r, t)$ is the probability that a CO molecule joins a particle at a distance r before it desorbs, and $\lambda = (D\tau_a)^{1/2}$ is the mean diffusion distance of a molecule, with D the diffusion coefficient and τ_a the mean residence time on the substrate.

With the boundary conditions $\varphi(\infty) = 0$ and $\varphi(r_0) = 1$ (each molecule reaching the particle edge is captured; r_0 is particle radius), the solution of Eq. (1) is given by

$$\varphi(r) = K_0(r/\lambda)/K_0(r_0/\lambda)$$

where K_0 is the modified Bessel function of zero order (*20*).

The mean flux of molecules reaching the particle (diameter ϕ) via the substrate is

$$f(r) = \int_{r_0}^{\infty} J_i \varphi(r) \pi r dr$$

where J_i is the incident flux of CO impinging on mica substrate

$$f'(r) = J_i \tau_a D \frac{w\pi r_0}{\lambda} K_1\left(\frac{r_0}{\lambda}\right) \Big/ K_0\left(\frac{r_0}{\lambda}\right)$$

and per unit area,

$$F_i = \frac{\lambda}{r_0} J_i K_1\left(\frac{r_0}{\lambda}\right) \Big/ K_0\left(\frac{r_0}{\lambda}\right).$$

K_1 is the modified first-order Bessel function.

We have plotted in Fig. 11 the values of F_i/J_i versus particle size ϕ for the two values of $\lambda = 2.5$ and 10 nm.

The total flux reaching a particle is $J_i + F_i$. Taking then into account this diffusion process, a particle of 4-nm diameter will receive a CO flux corresponding to 2 to 10 times the direct impinging flux J_i.

Table 3 gives, for samples from Fig. 7, both the F_i/J_i ratio and the actual s_0 values as calculated with an impinging flux equal to $F_i + J_i$. As a comparison the s_0 values corresponding to an incident flux J_i are also reported.

Assuming a diffusion distance of about 5 nm one can see that it is possible to obtain more accurate values for s_0.

Such a migration process should explain the change in CO oxidation rates as a function of particle size (*3*, *11*). In fact the

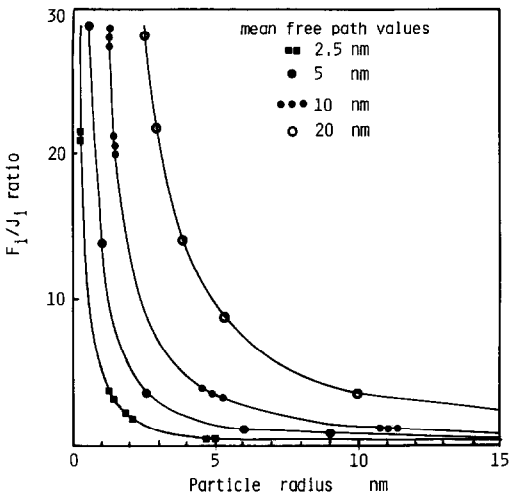

FIG. 11. Ratio F_i/J_i plotted versus particle size for various mean free path values. F_i and J_i are CO fluxes impinging on particles by diffusion on the mica substrate and from the atmosphere, respectively.

curves in Fig. 11 and the dCO_2/dt plots versus size in these references are quite similar.

Hence it is normal to assume that the same diffusion process producing an enhancement of impinging fluxes on the surface particles is responsible for the increase of both the turnover rate and the sticking coefficient, when the particle size decreases.

TABLE 3

Adsorption Kinetics for CO on Pd/Mica versus Particle Size

	$\bar{\lambda}$ (nm)	Average diameter (nm)		
		2.5	4	6.5
F_i/J_i	5	10	5	1
	2.5	4	2	0.5
s_0 as calculated with	5	0.9	0.92	0.85
$F_i + J_i$	2.5	1.8	1.83	1.13
s_0 calculated with J_i		9	5.5	1.7

Note. Comparison between initial sticking coefficient values (s_0) as calculated in two cases: (a) the impinging flux is the direct flux from the atmosphere, J_i; and (b) the impinging flux is the sum of J_i and the diffusion flux F_i. (Two values of the mean diffusion distance $\bar{\lambda}$ are envisaged, $\bar{\lambda}$ = 2.5 nm, and $\bar{\lambda}$ = 5 nm.)

CONCLUSIONS

TPD following CO chemisorption on well-defined supported Pd particles has shown two types of size effects:

(i) Very small particles (smaller than 5 nm) produce higher CO binding states than do larger particles, and during the desorption a part of the adsorbed population dissociates. These effects are suggested to be associated with the high proportion of edge sites on smaller particles.

(ii) Very large values of the initial sticking coefficient are found on small particles. This second size effect is interpreted with a migration process of CO molecules on the mica substrate.

REFERENCES

1. Gillet, M. F., and Channakhone, S., *J. Catal.* **97,** 427 (1986).
2. Thomas, M., Dickinson, J. T., Poppa, H., and Pound, G. M., *J. Vacuum Sci. Technol.* **15,** 568 (1978).
3. Ladda, S., Poppa, H., and Boudart, M., *Surf. Sci.* **102,** 151 (1981).
4. Doering, D. L., Poppa, H., and Dickinson, J. T., *J. Vacuum Sci. Technol.* **17,** 198 (1980).
5. Doering, D. L., Dickinson, J. T., and Poppa, H., *J. Catal.* **73,** 104 (1982).
6. Doering, D. L., Poppa, H., and Dickinson, J. T., *J. Catal.* **73,** 104 (1982).
7. Zhu, Y., and Schmidt, L. D., *Surf. Sci.* **129,** 107 (1983).
8. Takasu, Y., Unwin, R., Tesche, B., Bradshaw, A. M., and Grunze, M., *Surf. Sci.* **77,** 219 (1978).
9. Toolenaar, F. J. C. M., Bastein, A. G., and Ponec, V., *J. Catal.* **82,** 35 (1983).
10. Miquel, J. M., Thèse de 3ème Cycle, Université Aix-Marseille III, (1981).
11. Channakhone, S., Thèse de 3ème Cycle, Université Aix-Marseille III, (1984).
12. Nieuwenhuys, B. E., *Surf. Sci.* **126,** 307 (1983).
13. Weinberg, W. H., Comrie, C. M., and Lambert, R. M., *J. Catal.* **41,** 489 (1976).

14. Cassuto, A., and King, D. A., *Surf. Sci.* **102,** 388 (1981).
15. Zhdanov, V. P., *Surf. Sci.* **133,** 469 (1983).
16. Alnot, M., and Cassuto, A., *Surf. Sci.* **112,** 325 (1981).
17. Schmick, M. D., and Wassmuth, M. W., *Surf. Sci.* **123,** 471 (1982).
18. Conrad, M., Ertl, G., Koch, J., and Latta, E. E., *Surf. Sci.* **43,** 462 (1974).
19. Matolin, V., Gillet, E., and Channakhone, S., *J. Catal.* **97,** 448 (1986).
20. Lewis, B., and Anderson, J. C., Nucleation and Growth of Thin Films," p. 34. Academic Press, New York, 1978.